Plant Physiology®

Research Article

Protection of photosystem I during sudden light stress depends on ferredoxin:NADP(H) reductase abundance and interactions

Melvin Rodriguez-Heredia,[1] Francesco Saccon (ID),[1] Sam Wilson,[1] Giovanni Finazzi (ID),[2] Alexander V. Ruban (ID)[1] and Guy T. Hanke (ID)[1,*,†]

1   Department of Biochemistry, Queen Mary University of London, London E1 4NS, UK
2   Laboratoire de Physiologie Cellulaire et Végétale, UMR 5168, Centre National de la Recherche Scientifique (CNRS), Commissariat à l'Energie Atomique et aux Energies Alternatives (CEA), Université Grenoble Alpes, Institut National de Recherche Agronomique (INRA), Institut de Recherche en Sciences et Technologies pour le Vivant (iRTSV), CEA Grenoble, F-38054 Grenoble cedex 9, France

*Author for communication: g.hanke@qmul.ac.uk
†Senior author

Abstract

Plant tolerance to high light and oxidative stress is increased by overexpression of the photosynthetic enzyme Ferredoxin:NADP(H) reductase (FNR), but the specific mechanism of FNR-mediated protection remains enigmatic. It has also been reported that the localization of this enzyme within the chloroplast is related to its role in stress tolerance. Here, we dissected the impact of FNR content and location on photoinactivation of photosystem I (PSI) and photosystem II (PSII) during high light stress of Arabidopsis (*Arabidopsis thaliana*). The reaction center of PSII is efficiently turned over during light stress, while damage to PSI takes much longer to repair. Our results indicate a PSI sepcific effect, where efficient oxidation of the PSI primary donor (P700) upon transition from darkness to light, depends on FNR recruitment to the thylakoid membrane tether proteins: thylakoid rhodanase-like protein (TROL) and translocon at the inner envelope of chloroplasts 62 (Tic62). When these interactions were disrupted, PSI photoinactivation occurred. In contrast, there was a moderate delay in the onset of PSII damage. Based on measurements of ΔpH formation and cyclic electron flow, we propose that FNR location influences the speed at which photosynthetic control is induced, resulting in specific impact on PSI damage. Membrane tethering of FNR therefore plays a role in alleviating high light stress, by regulating electron distribution during short-term responses to light.

Introduction

Electrons excited at photosystem I (PSI) reduce ferredoxin (Fd), and the majority of these are used by the enzyme Fd:NADP(H) oxidoreductase (FNR) to generate NADPH (Shin et al., 1963), which is required for CO_2 fixation. In Angiosperms, FNR is tightly bound to the thylakoid membrane tethers thylakoid rhodanase-like (TROL) protein and

Open Access

translocon at the inner envelope of chloroplasts 62 (Tic62) in the dark (Juric et al., 2009; Benz et al., 2010; Yang et al., 2016), but this association is weakened at higher pH in vitro, and in the light (Alte et al., 2010). Association of FNR with PSI is also reported (Andersen et al., 1992; Marco et al., 2019), and based on immunogold labeling it was proposed that FNR released from the Tic62/TROL tethers in the presence of light could be localized at PSI (Kramer et al., 2021). Oxidized PSI is re-reduced with electrons from plastocyanin (Hippler and Drepper, 2006), which shuttles them through the thylakoid lumen from the cytochrome b_6f complex (Cyt b_6f). The Cyt b_6f is reduced in turn by plastoquinol (PQH_2), which is the electron acceptor at photosystem II (PSII). This plastoquinone (PQ) reduction and oxidation drives formation of ΔpH, which is used by the thylakoid ATPase to synthesize ATP.

Photoexcitation of PSI can alternatively be used to form ΔpH by returning electrons from Fd to PQ through at least two cyclic electron flow (CEF) pathways (Munekage et al., 2004). One Fd:PQ reductase is a homolog of respiratory complex I, known as the NDH (Burrows et al., 1998; Shikanai et al., 1998; Yamamoto and Shikanai, 2013), while the mechanism of the other Fd:PQ reductase, which is inhibited by antimycin A (AA), remains enigmatic (Munekage et al., 2002; Fisher and Kramer, 2014; Nawrocki et al., 2019). Proposed mechanisms involve the function of the proton-gradient regulation 5 (Pgr5) and Pgr5 like 1 (PgrL1) proteins (Munekage et al., 2002; Hertle et al., 2013) and/or direct electron donation from Fd or even FNR to PQ at the Cyt b_6f (Zhang et al., 2001; Nawrocki et al., 2019; Sarewicz et al., 2021). FNR has also been co-purified with the Cyt b_6f (Clark et al., 1984; Zhang et al., 2001) and interaction is reported with PgrL1 (DalCorso et al., 2008). We have recently reported that FNR binding to the thylakoid through either the TROL or Tic62 membrane tethers is necessary for CEF when Arabidopsis (Arabidopsis thaliana) plants are transferred from the dark to the light (Kramer et al., 2021), a condition in which CEF is upregulated (Joliot and Joliot, 2006).

Production of damaging reactive oxygen species (ROS) increases in the absence of acceptors at either photosystem. If PQ availability at PSII is limiting, excitation is transferred from triplet-state chlorophyll to O_2, producing dangerous singlet oxygen ($^1O_2$) (Telfer et al., 1994; Krieger-Liszkay, 2005). This occurs even at very low light, and the reaction center subunit of PSII (D1) is constantly turned over to ensure functional PSII (Fufezan et al., 2002). To minimize such damage, excitation at PSII can be dissipated through non-photochemical quenching (NPQ) mechanisms induced by acidification of the thylakoid lumen (Ruban, 2016; Ruban and Wilson, 2020). Upregulation of this thermal dissipation in vivo requires the PsbS protein and de-epoxidation of the xanthophyll pigment violaxanthin into zeaxanthin, both of which are triggered by the formation of ΔpH (Ware et al., 2015; Sacharz et al., 2017; Steen et al., 2020; Saccon et al., 2020a, 2020b).

If oxidized Fd availability at PSI is limiting, excited electrons are passed from the iron–sulfur (FeS) clusters at the stromal side of PSI to oxygen, forming superoxide ($O_2^{\bullet-}$) (Allen and Hall, 1974), which is rapidly dismutated enzymatically to hydrogen peroxide (H_2O_2) (Asada, 1999). This H_2O_2 can be converted to hydroxyl radicals ($^\bullet OH$) through Fenton chemistry, a process catalyzed by the PSI FeS clusters in their reduced state, resulting in their rapid destruction by the resulting $^\bullet OH$ (Sonoike et al., 1995; Sonoike, 2011). Degradation of the PSI reaction center subunits quickly follows (Ivanov et al., 1998; Tjus et al., 1998) and this requires costly reconstruction of the entire photosystem, which can take days (Kudoh and Sonoike, 2002; Lima-Melo et al., 2019a, 2019b). In angiosperms, this is prevented by restricting electron donation to PSI, maintaining the P700 active center and FeS clusters in an oxidized state (Shimakawa and Miyake, 2019; Storti et al., 2020). PSI donor limitation is promoted either through downregulation/damage to PSII (Ivanov et al., 1998; Tikkanen et al., 2014; Chaux et al., 2015), or through "photosynthetic control" in which PQH_2 oxidation at the Cyt b_6f is limited by high ΔpH (Tikkanen et al., 2015; Colombo et al., 2016). It has been reported that the role of CEF in photoprotection is related to enhanced generation of ΔpH to induce protective mechanisms, rather than providing alternative PSI acceptors (Rantala et al., 2020).

Experiments on transgenic Nicotiana tabacum (tobacco), with FNR either over-expressed or knocked down by antisense, showed that FNR abundance corresponded with tolerance to high light and oxidative stress, and considerable damage at PSII was detected when FNR contents were low (Palatnik et al., 2003; Rodriguez et al., 2007). It was hypothesized that FNR could be affording protection through its role as a PSI acceptor, preventing build-up of electrons in the thylakoid and possibly acting as a diaphorase to remove radical species. We previously found that FNR could generate considerable $O_2^{\bullet-}$ during turnover, and that stress remediation pathways were upregulated in Arabidopsis over-expressing FNR (Kozuleva et al., 2016). We interpreted this as indicating the enzyme might confer stress tolerance by "priming" the plant to induce increased abundance of proteins involved in protective mechanisms, such as superoxide dismutation, prior to stress exposure. FNR:membrane complex associations are also implicated in stress responses. It has been shown that FNR is released from the thylakoid during oxidative stress (Palatnik et al., 1997), and plants with different FNR:membrane associations also vary in stress responses (Lintala et al., 2009, 2012; Kozuleva et al., 2016).

There has been much recent research on PSI photoinhibition, a considerable amount relating to how processes in the post-PSI electron transfer cascade can relieve acceptor limitation and prevent damage (Shimakawa and Miyake, 2018a, 2018b; 2019; Lima-Melo et al., 2019a, 2019b; Leister, 2020; Storti et al., 2020). However, there are no reports of how this might relate to FNR abundance or location, despite the fact that FNR abundance strongly corresponds to stress tolerance (Palatnik et al., 1997, 2003; Rodriguez et al., 2007; Kozuleva et al., 2016). In the work presented here, we dissect the impact of changing FNR content and sub-chloroplast

location on PSI and PSII. We find that when plants with perturbed FNR:membrane interactions are exposed to sudden high light, there is specific photoinactivation of PSI. Dark recovery after illumination shows that PSI damage correlates with this inactivation. Surprisingly, over the same timescale, PSII is slightly less photodamaged than in the wild-type (WT) as measured by fluorescence quenching in the dark (qPd). Protection of PSI correlates with CEF capacity, the rate of proton gradient (ΔpH) generation and is AA dependent, but PsbS-mediated NPQ has a minimal effect on PSI photoprotection. It is suggested that protection at PSI may contribute to the stress tolerance conferred by FNR.

Results

Estimating PSI photoinactivation and PSII photoinhibition during illumination

In order to differentiate between impact at PSII and PSI during the illumination period, we first established high light treatment protocols. To estimate the onset of damage at PSII, we measured PSII capacity as Y(II) (Schreiber and Klughammer, 2009) and the value of photochemical qPd, which incorporates a comparison between actual and theoretical F_0 values (Ruban and Murchie, 2012; Ruban, 2017) to identify the early stages of PSII photodamage. We also defined a protocol to estimate PSI capacity during illumination. Although measurement of PSI capacity in plants following dark adaptation (Pm) is well established (Yamori et al., 2016; Shimakawa and Miyake, 2018a, 2018b; Rantala et al., 2020), this is hard to accurately determine during illumination. We followed the protocol of Klughammer and Schreiber (2008), by briefly turning off the actinic light while applying a 10 s far-red (FR) light pulse prior to a saturating flash. Here, we call this transient P700 maximum (tPm) to help differentiate it from the Pm values calculated following prolonged dark adaptation/recovery.

To examine whether decreases in PSI capacity measured during illumination (tPm) translate into photodamage as calculated by Pm, we compared *A. thaliana* WT with a classic genetic model prone to PSI damage, the *pgr5* mutant (Takagi and Miyake, 2018; Rantala et al., 2020; Storti et al., 2020). The tPm is relatively similar in *pgr5* and the WT for the first 5 min of high light (Figure 1), as it drops from 1 to around 0.78. Thereafter, the WT stabilizes at around 0.75, while *pgr5* continues by decreasing further to around 0.35. Some recovery is seen in both genotypes following 30 min in the dark (to 0.85 for the WT and 0.4 for *pgr5*), indicating a component of the decrease in tPm is not related to PSI damage. For this reason, throughout the text, we refer to decreases in tPm as PSI photoinactivation, as it contains a recoverable component, while decreases in Pm following dark relaxation are described as photodamage. A significant ~0.4 difference between WT and *pgr5* values is consistent between the final tPm and the dark recovered Pm. This confirms the predisposition of *pgr5* to PSI photodamage, and indicates that differences between WT and *pgr5* tPm values are predominantly due to PSI damage. Therefore, at least in
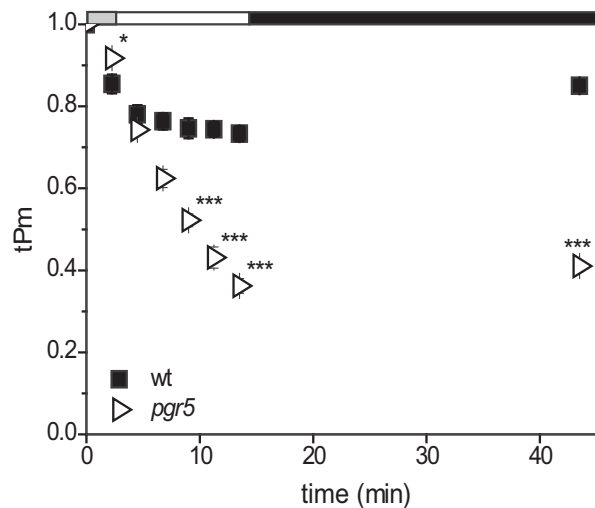

Figure 1 Suitability of the tPm parameter to follow PSI inactivation during the light. Timing of the changes in light intensity is indicated above the graph: The grey bar indicates a step-wise increase to first 543, then 692 µmol photon m^{-2}s^{-1} (1 min each). The white bar indicates continuous illumination at 1,385 µmol photon m^{-2}s^{-1}, and the black bar indicates a dark relaxation period. WT (black squares) and *pgr5* (open right-pointing triangles). tPm was measured upon illumination. Absolute Pm was determined after 30 min of dark adaptation. Data shown are mean ± SEM ($n \geqslant 3$ individuals per genotype). Differences attributed by post hoc honest significant difference Tukey's test. P values are indicated as "***" < 0.001, "**" < 0.01, "*" < 0.05, "." < 0.1.

these conditions, tPm can provide an estimate of real-time PSI photodamage, and this also confirms that damage to PSI (a decrease in PSI activity by ~15% after dark recovery) can be achieved in WT Arabidopsis through the application of 15 min of high light.

FNR abundance and location are related to PSI inactivation

As a first step to investigating the relationship between FNR and photoinactivation at PSI and PSII, we analyzed the *fnr1* knockout mutant of FNR1 in Arabidopsis, which has increased susceptibility to high light stress (Kozuleva et al., 2016). This was done over gradually increasing light intensity to allow induction of PSII photoprotective mechanisms (Wilson and Ruban, 2019, 2020). Measurements of tPm (Figure 2A) showed greater photoinactivation of PSI in *fnr1*, both at low and high light intensities. The PSI quantum yield, Y(I), was decreased in *fnr1* relative to the wt at lower light intensities (Figure 2B). As expected for a mutant lacking ~50% of FNR (a component involved in acceptor regeneration at PSI), the *fnr1* genotype showed significantly greater acceptor limitation, Y(NA), than the WT (Figure 2C). Surprisingly, the *fnr1* genotype shows slightly less photodamage to PSII, as indicated by higher qPd and Y(II) values than WT plants (Figure 2, D and E), although only Y(II) showed statistical significance.

The *fnr1* plants not only lack around 50% of the WT FNR, but also additionally show a change in the location of the
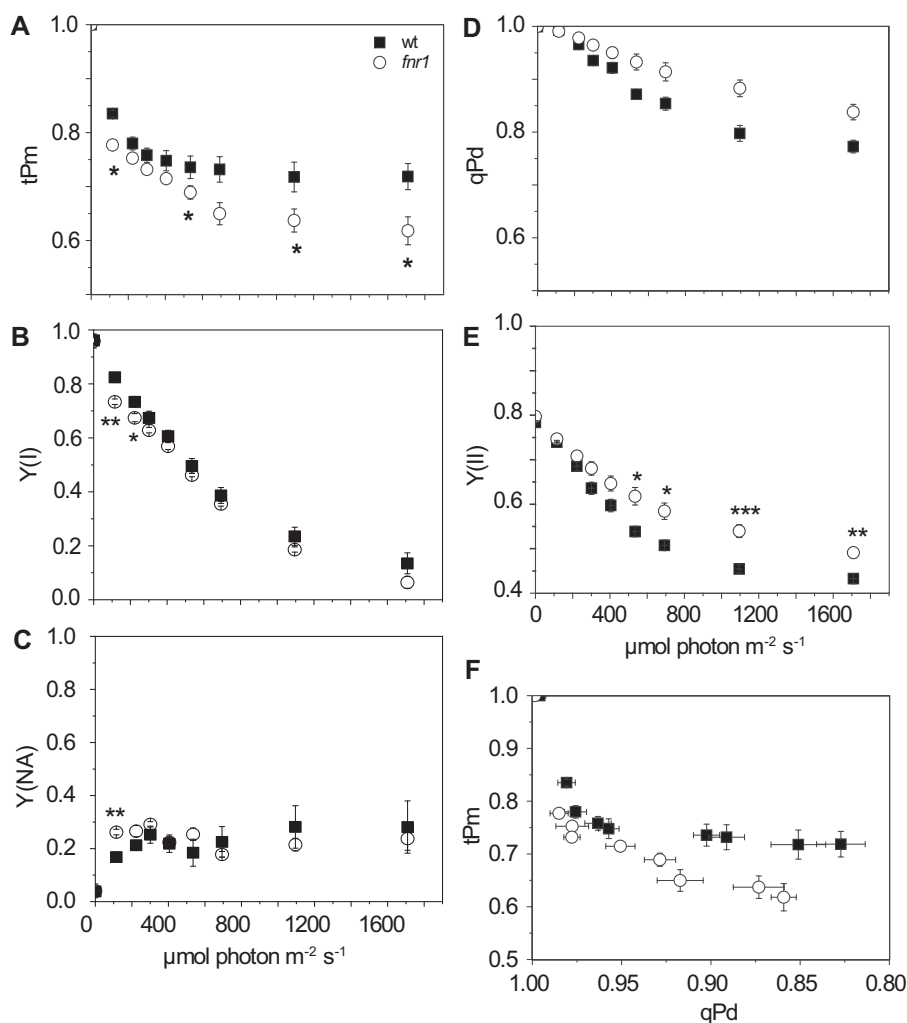
Figure 2 A comparison of PSI and PSII inactivation over increasing light intensity in WT (black squares) and *fnr1* (open circles). A, tPm. B, Effective quantum yield of PSI (Y(I)). C, acceptor limitation at PSI (Y(NA)). D, photochemical quenching of PSII in the dark (qPd). E, Effective quantum yield of PSII (Y(II)). F, Relationship between tPm and qPd. Data shown are mean ± SEM (n = 5–7 individuals per genotype). Differences attributed by post hoc honest significant difference Tukey's test. P values are indicated as "***" < 0.001, "**" < 0.01, "*" < 0.05, "." < 0.1.

remaining enzyme (Lintala et al., 2007; Hanke et al., 2008), due to low interaction with Tic62 and TROL (Benz et al., 2010). To understand whether the phenotype of *fnr1* is due to decreased FNR content or altered FNR interactions, we analyzed the *tic62/trol* double mutant, which lacks both FNR:membrane tether proteins. The *tic62/trol* mutant retains higher levels of FNR than the *fnr1* mutant, although still less than the WT (Lintala et al., 2014). Relative to the WT, *tic62/trol* and *fnr1* show a similar decrease in tPm (Figure 3A), which becomes significant at higher light intensities, although the PSI acceptor limitation is much lower in *tic62/trol* (Figure 3C). Similar increases in qPd and Y(II) are also seen between the genotypes (Figure 3, D and E). To compare real-time photoinactivation at PSI and photodamage to PSII, we plotted qPd against tPm (Figures 2, F and 3, F). Although there appears to be a negative correlation between tPm and qPd, this is unlikely to be causative, because the parameters show poor correlation in the WT, *fnr1* and *tic62/trol* genotypes (R^2 = 0.330, 0.451, and 0.512, respectively).

Both *fnr1* and *tic62/trol* plants have disrupted FNR:tether protein interaction and decreased total FNR content. To try and distinguish the impact of FNR interactions from FNR abundance, we exploited plants in which the *fnr1* mutant was complemented with genes for FNR proteins that specifically interact with TROL (ZmFNR1), Tic62 (ZmFNR2) and only show weak interaction with either tether (ZmFNR3) (Twachtmann et al., 2012; Kramer et al., 2021). Chloroplasts of these plants previously showed equivalent FNR immunostaining to the WT (Kramer et al., 2021). We aimed to use the *fnr1*:Zm*FNR3* line to establish whether WT levels of enzyme, weakly bound to the Tic62/TROL tethers could prevent the decreased tPm seen in *fnr1* and *tic62/trol*. Because antigenicity of iso-proteins may vary, we confirmed that NADPH dependent Fd reduction activity of leaf crude extracts was roughly equivalent between WT (0.26 μmol^{-1} μg protein^{-1} s ± 0.002 SD) and *fnr1*:Zm*FNR3* (0.24 μmol^{-1} μg protein^{-1} s ± 0.014 SD). On increasing light intensities, the PSI parameters of *fnr1*:Zm*FNR3* did not fully recover to WT
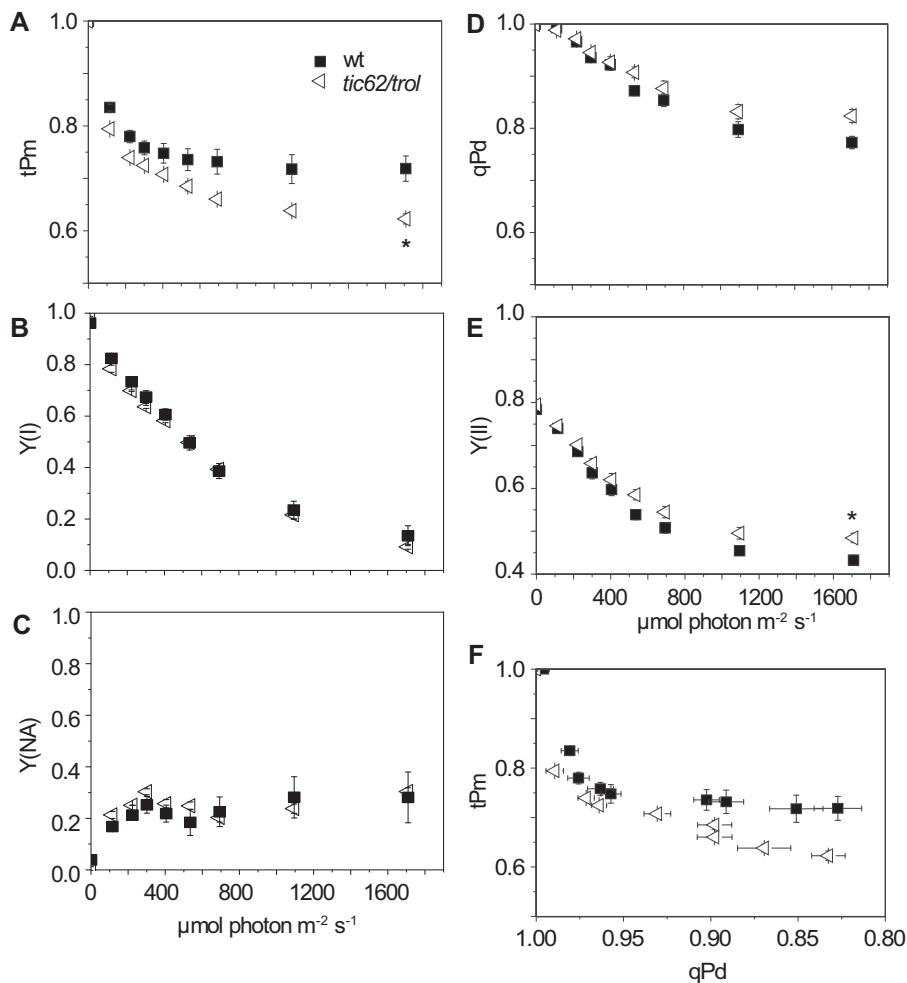
Figure 3 A comparison of PSI and PSII inactivation over increasing light intensity in WT (black squares) and *tic62/trol* (open left-pointing triangles). A, tPm. B, Effective quantum yield of PSI (Y(I)). C, Acceptor limitation at PSI (Y(NA)). D, qPd. E, Effective quantum yield at PSII (Y(II)). F, Relationship between tPm and qPd. Data shown are means $\pm$ SEM (n = 5–7 individuals per genotype). Differences attributed by post hoc honest significant difference Tukey. P values indicated by "***" < 0.001, "**" < 0.01, "*" < 0.05, "." < 0.1.

levels, although this was not statistically significant, and developed significantly higher Y(II) values (Supplemental Figure S1). This similar profile of *fnr1*:Zm*FNR3* to *tic62/trol* and *fnr1* indicates that membrane tether association might indeed be related to the relationship between FNR and stress tolerance. By contrast, Supplemental Figure S1 shows that *fnr1*:Zm*FNR1* and *fnr1*:Zm*FNR2*, which interact strongly with TROL and Tic62, respectively, were almost identical to the WT in terms of tPm, Y(I), qPd, and Y(II).

PSI photoinactivation is partly independent of acceptor limitation

To further probe the relationship between stress tolerance and FNR:membrane tether interactions, we selected three specific genotypes for further experiments: WT; the *tic62/trol* mutant, which lacks FNR:membrane tether interactions; and the *fnr1*:Zm*FNR1* line, which contains WT levels of FNR and increased FNR:TROL interaction (Kramer et al., 2021).

Interaction of FNR with TROL is stronger than Tic62 (Alte et al., 2010), so *fnr1*:Zm*FNR1* has exaggerated FNR:tether binding in comparison to the WT.

These genotypes were then subjected to a sudden application of high light (as in Figure 1) to promote rapid PSI damage. Figure 4A shows that tPm values were significantly lower in the *tic62/trol* mutant over the high light treatment (Figure 4A). This is despite the fact that Y(NA) values indicate acceptor limitation does not vary between WT and *tic62/trol* (Figure 4C). In contrast to the *pgr5* mutant (Figure 1), PSI inactivation occurred rapidly during the initial part of the treatment. Importantly, the statistically significant ~0.1 difference between WT and *tic62/trol* tPm values over illumination is also seen in the Pm values, measured after a 30-min dark recovery. This indicates that the difference between WT and *tic62/trol* tPm values is due to increased photodamage at PSI. Although FNR content in the *tic62/trol* mutant is greater than the *fnr1* mutant, it is still decreased in comparison to the WT (Lintala et al., 2014). As a further
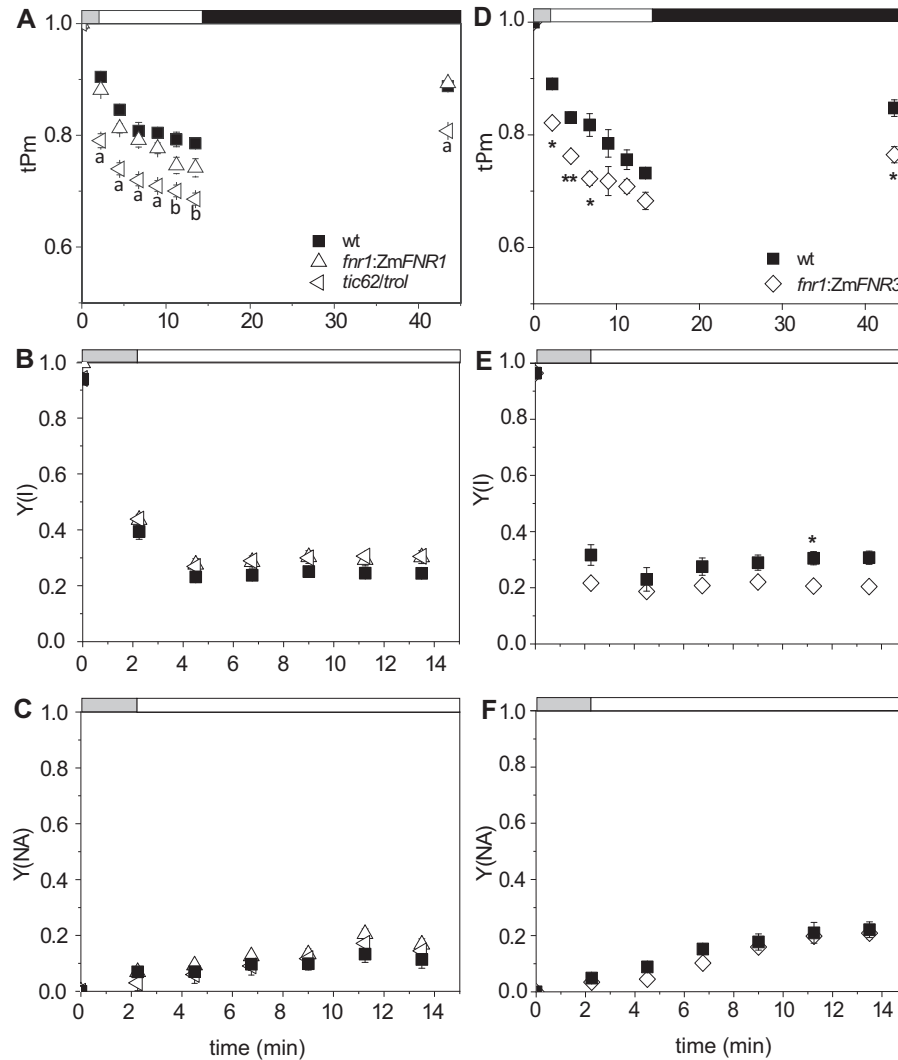
Figure 4 The impact of (FNR:tether interactions on PSI photoinactivation. A–C, Compared 4-week-old WT (black squares), *fnr1*:Zm*FNR1* (open upward-pointing triangles), and *tic62/trol* (open left-pointing triangles) plants. D and E, Compared 6-week-old WT (black squares) and *fnr1*:Zm*FNR3* (open diamonds) plants. Timing of changes in light intensity is indicated above the graph: the gray bar indicates a step-wise increase to first 543, then 692 µmol photon m^{-2}s^{-1} (1 min each). The white bar indicates continuous illumination at 1,385 µmol photon m^{-2}s^{-1}, and the black bar indicates a dark relaxation period. A and D, tPm was measured over illumination. Absolute Pm was determined after 30 min of dark adaptation. B and E, Effective quantum yield of PSI (Y(I)). C and F, Acceptor limitation at PSI (Y(NA)). A–C, Data shown are means ± SEM ($n \geqslant 3$ individuals per genotype). Significant differences were attributed by post-hoc honestly significant difference Tukey Test and *P* values < 0.05 are indicated as the following letters: "a" for WT, *fnr1*:Zm*FNR1* ≠ *tic62/trol*; "b" for WT ≠ *tic62/trol*. D–F, Differences from WT attributed by Student's *t* test. *P* values indicated by "***" < 0.001, "**" < 0.01, "*" < 0.05, "." < 0.1.

control to distinguish between the impact of decreased total FNR dose and decreased FNR:Tic62/TROL interactions, we also tested the *fnr1* mutant line complemented with maize FNR3, which has a low affinity for TROL and Tic62. Interestingly, treatment of *fnr1*:Zm*FNR3* with sudden high light resulted in significantly decreased tPm values relative to WT within 1 min (Figure 4D). As in the case of the *tic62/trol* mutant, there was no difference in PSI acceptor limitation as measured by Y(NA) for either *fnr1*:Zm*FNR3* (Figure 4F) or the *fnr1* mutant (Supplemental Figure S2). This confirms that the impact of FNR:tether interactions on PSI photodamage is at least partly independent of acceptor limitation.

FNR abundance and location are important for CEF and ΔpH generation

Apart from preventing acceptor limitation at PSI, another mechanism by which FNR could prevent photoinactivation is through a role in CEF, to restrict electron supply to PSI. We have recently shown that short-term induction of CEF on transfer from dark to light is dependent on FNR:tether interactions (Kramer et al., 2021). This data showed that the *fnr1* mutant lost CEF capacity, and that this could be rescued by expression of Zm*FNR1* (strong TROL binding) but not Zm*FNR3* (weak tether interactions). We, therefore, compared relative CEF capacity of WT and the *tic62/trol* mutant following either dark adaptation, or light acclimation (Figure

5A). CEF is elevated in the WT after dark adaptation as previously reported (Kramer et al., 2021), but not in the *tic62/trol* mutant. CEF has the capacity to accelerate generation of ΔpH and we therefore compared the rate at which ΔpH is generated at the onset of light. Initially, 312 µmol photon m^{-2} s^{-1} was used, and we confirmed that this light intensity was saturating by repeating the experiment at 586 µmol photon m^{-2} s^{-1} (Figure 5B). Dark-adapted chloroplast preparations from WT, *fnr1*:Zm-*FNR1*, and *tic62/trol*, had equivalent F_v/F_m values of 0.74 ± 0.01, 0.72 ± 0.04, and 0.70 ± 0.03, respectively, indicating that chloroplasts were of equivalent quality. We found no significant difference between the amplitude of fluorescence quenching of the three genotypes. However, we observed a ~30% increase in the half time to reach maximum fluorescence quenching in *tic62/trol* compared to the WT and *fnr1*:Zm*FNR1* (Figure 5C) at both irradiance intensities. As the same genotype shows an inability to upregulate CEF on dark adaptation, caused by disruption of FNR:tether interactions, it is highly likely that the decreased rate of ΔpH development upon transitions from darkness to light is due to a missing contribution of CEF to proton pumping. To further investigate whether an inability to upregulate CEF on transition to higher light results in the decreased tPm values measured in the *tic62/trol* and *fnr1*:Zm*FNR3* plants, we examined the impact of the classical CEF inhibitor AA on tPm. Figure 5D shows that infiltration of leaves with 5 µM AA is sufficient to eliminate the difference in tPm between WT and *fnr1*:Zm*FNR3*, while the difference between WT and *tic62/trol* ceases to be significant. Infiltration with methyl viologen (MV), which should compete with FNR for reduced electrons, also eliminates this difference but only on a longer timescale.

Faster development of ΔpH might accelerate PSI oxidation, and therefore protection, by inducing PsbS-dependent NPQ to limit the flux of electrons from PSII (Tikkanen et al., 2014; Chaux et al., 2015). We, therefore, compared how NPQ induction over increasing light intensities influenced inactivation of PSI (tPm). Figure 6 shows that there is no significant difference in NPQ values between the genotypes, and that tPm does not correlate with NPQ development over increasing light intensity. To further evaluate whether PsbS-dependent NPQ might play a role in protecting PSI from photoinactivation in Arabidopsis, we also measured genotypes with enhanced NPQ (*L17*) (Li et al., 2002), or compromised NPQ (*npq4*) (Havaux and Niyogi, 1999; Figure 6), confirming that, under these conditions at least, there is no relationship between NPQ and tPm. We further treated these genotypes with the sudden high light protocol (Supplemental Figure S3, C–E) which resulted in similar tPm and final Pm values for WT, *L17*, and *npq4*. This result suggests that NPQ does not limit PSI re-reduction in either condition measured here.

Any mechanistic role of FNR in CEF remains unclear. To compare the impact of FNR:Tic62/TROL interaction with the classical pathways of CEF, we used the same protocol to check whether a similar response could be measured in *pgr*5

(a mutant of the Pgr5/PgrL1 pathway, as shown in Figure 1) and *crr*2 (an assembly factor mutant of the NDH complex). In Figure 7, neither of these mutants show a similar pattern of PSI inactivation to *tic62/trol*, *fnr1*, or *fnr1*:Zm*FNR3* plants. On sudden high light illumination of *pgr5*, tPm is initially higher than in WT and then gradually decreases over the time course, to much lower values than other genotypes (Figure 7A), while *crr*2 also shows higher initial tPm values than WT, but does not decrease below WT values. Y(NA) values indicate increased acceptor limitation relative to wt for both *pgr*5 and *crr*2 (Figure 7C). Interestingly, when these genotypes are subject to an increasing light protocol (Supplemental Figure S4) *crr*2 plants present higher tPm values than the WT up to light intensities of 1,096 µmol photons m^{-2} s^{-1}.

FNR impact on PSI photoinactivation upon fluctuating light

It has been frequently reported that fluctuating light exacerbates the damage to PSI caused by perturbation of CEF (Suorsa et al., 2012, 2013; Kono et al., 2014; Huang et al., 2018; Nikkanen et al., 2018), and we therefore repeated our experiment using a fluctuating light environment. This comprised three phases of high light (1385 µmol photon m^{-2} s^{-1}) intensity illumination alternating with total darkness (Figure 8). Following the first light treatment, tPm values were lower for the *tic62/trol* mutant throughout the illumination protocol (Figure 8A). When measured during illumination periods, genotype had no effect on PSI yield and acceptor limitation (Figure 8B, Figure 8C). There were significantly lower Y(I) and higher Y(NA) values for *tic62/trol* following the dark steps. The final Pm values were lower after this fluctuating light routine (Figure 8A) relative to those obtained after continuous high light (Figure 4A) in all the genotypes. Interestingly, the dark recovery of *Pm* only decreased by ~9% in *fnr1*:Zm-*FNR1* which, unlike the WT, retained a significant difference from *tic62/trol*.

Discussion

We hypothesized that, as FNR is a critical component of the post-PSI electron transfer cascade, its abundance, and/or location on the membrane (close to PSI), might contribute to PSI protection. This could be analogous to the impact of the flavodiiron proteins (Shimakawa et al., 2017; Alboresi et al., 2019), or photorespiration (Allahverdiyeva et al., 2011; Hanawa et al., 2017; Takagi et al., 2017), providing excess sinks to maintain P700 in a protected, oxidized state. Because differences in electron transport induced by altered FNR content or location are most pronounced in the early stages of illumination following dark adaptation (Twachtmann et al., 2012; Kramer et al., 2021), it was critical to estimate PSI inactivation during the early stages of illumination, for which we used the tPm parameter (Figure 1). This revealed that, over the relatively short high light stress applied here, FNR content and membrane association specifically
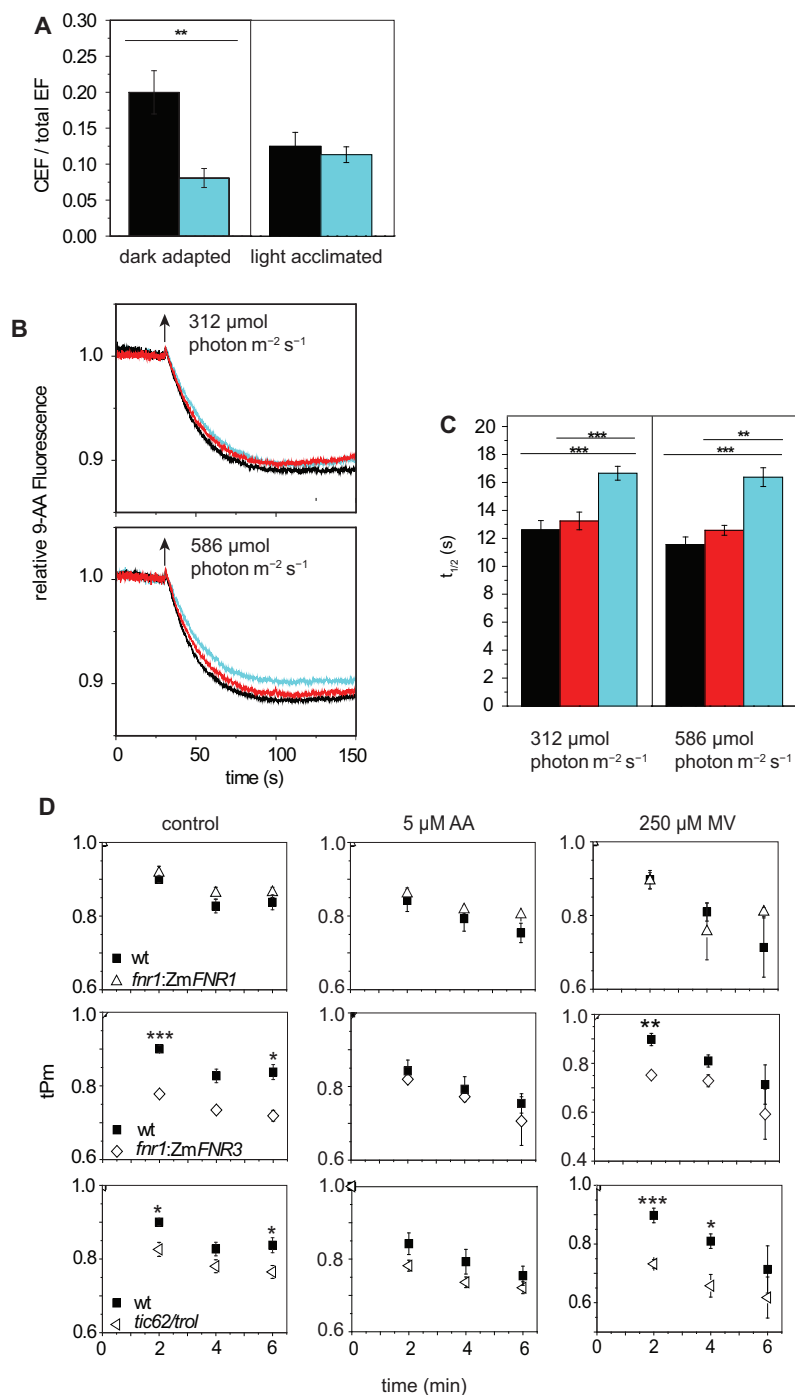
Figure 5 The impact of :FNR:tether interactions on CEF and generation of ΔpH. Genotypes are: WT (black), *fnr1*:Zm*FNR1* (red) and *tic62/trol* (cyan). A, Comparison of the maximum rate of leaf CEF as a function of total electron flow. Values calculated from ECS measurements following a 20 s high light pulse (actinic light for total electron flow, FR light for CEF). Means of measurements on three to five individuals per genotype ± SEM. Light acclimation was for 5 min at 150 μmol photons m^{-2}s^{-1}. B, ΔpH generation by isolated chloroplasts, measured by 9-AA fluorescence quenching. Onset of actinic irradiance is indicated by upward arrow. Irradiance at 312 (upper graph) and 586 μmol photon m^{-2}s^{-1} (lower graph). Traces are averages of three independent experiments. C, Rate of ΔpH generation, calculated as $t_{1/2}$ on illumination at the indicated light intensities. Values are means ± SEM of experiments on three independent chloroplast preparations for each genotype. Differences attributed by post-hoc honestly significant difference Tukey's test for half times for rate of ΔpH generation and Student *t* test for CEF analysis. *P* values are indicated as "***" < 0.001, "**" < 0.01, "*" < 0.05, "." < 0.1. D, Impact of inhibitors on tPm determination following sudden illumination at 1,095 μmol photon m^{-2} s^{-1}. Individual leaves were dark-adapted for 40 min and infiltrated with buffer, 5 μM AA or 250 μM MV, prior to illumination and measurement of tPm at the indicated times. Data are means ± SEM ($n \geqslant 3$ individuals per genotype). Differences from WT values attributed by Student's *t* test. *P* value indicated by "***" < 0.001, "**" < 0.01, "*" < 0.05.
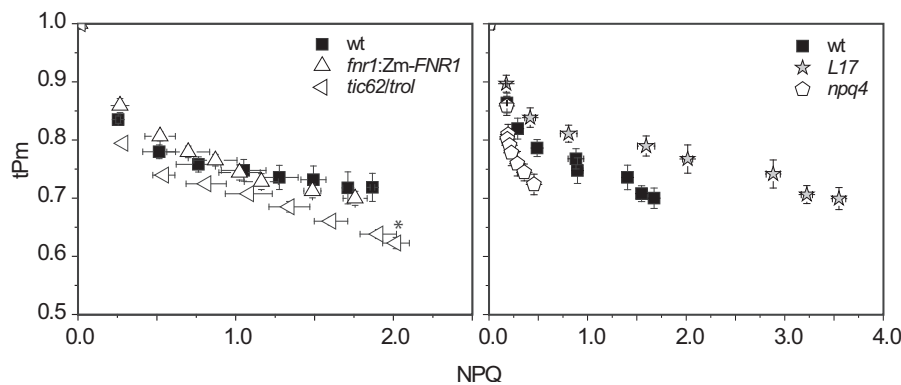
Figure 6 Examining a role for NPQ in FNR dependent protection of PSI. Increasing actinic light intensity was applied to plants and tPm and NPQ parameters calculated as described in "Materials and methods". Genotypes in the left panel are WT (black squares), *fnr1*:Zm*FNR1* (open upward-pointing triangles), *tic62/trol* (open left-pointing triangles). Genotypes in the right panel are *L17* (gray stars) and *npq4* (open pentagons). Data shown are means ± SEM ($n \geqslant 3$ individuals per genotype). Significant differences were attributed by post-hoc honestly significant difference Tukey's test. Only tPm differences are indicated on this Figure: P values are indicated as "***" < 0.001, "**" < 0.01, "*" < 0.05, "." < 0.1. See Supplemental Figure S3 for original NPQ and tPm values plotted against light intensity.

impact on photoinactivation of PSI. Interestingly, the increased PSI photoinactivation in *fnr1*, *fnr1*:Zm*FNR3*, and *tic62/trol* mutants occurs at the same time as a small, but significant improvement in PSII protection.

PSI acceptor limitation is associated with $O_2^{\bullet -}$ generation (Takahashi and Asada, 1988; Kozuleva et al., 2014), and FNR can also generate $O_2^{\bullet -}$ during catalysis (Kozuleva et al., 2016). Perhaps surprisingly, detection of light-dependent free radical evolution in antisense tobacco leaves indicated that decreased FNR content resulted in no difference in $O_2^{\bullet -}$, but rather an increase in $^1O_2$ (Palatnik et al., 2003), a radical normally associated with PSII damage. In addition, spin-trapping of $O_2^{\bullet -}$ produced by chloroplasts from Arabidopsis single *trol* knockout plants was previously shown to be lower than in WT in both light and dark (Vojta et al., 2015). The results in tobacco prompted the suggestion that PSII was acceptor limited, due to back up of electrons through the whole electron transport chain (Palatnik et al., 2003). This might not be contradictory to our data, as the light stress applied to tobacco FNR antisense plants prior to measurement was for much longer time scales than used in our study. Our data (Figures 2–4 and 8; Supplemental Figures S1 and S2) indicate that the FNR associated PSI photoinactivation occurs early in illumination. In the absence of correct FNR:tether interaction, poor initial regulation of events around PSI on illumination, or an increase in light intensity, may therefore cause a temporary increase in $O_2^{\bullet -}$ (and therefore $^{\bullet}OH$) production relative to the WT. PSI damage would then progress from the destruction of FeS clusters to protein subunits at a small percentage of PSI complexes, resulting in $^1O_2$ production from triplet state chlorophyll at damaged PSI (Sonoike et al., 1995; Tjus et al., 1998). PSII is highly sensitive to $^1O_2$ (Krieger-Liszkay, 2005) and so a small amount of PSI damage could result in considerable PSII damage (Sonoike, 2011). The small, short-term improvement in PSII tolerance to high light stress seen in plants with disrupted FNR:tether interactions might have a number of causes. These include secondary effects to decrease light harvesting or increase PQ

acceptor availability at PSII in response to the direct impact at PSI, and are beyond the scope of this study.

We expected that the main impact of FNR abundance and/or location on PSI damage would relate to acceptor limitation. However, our results indicate that the effect is more complex. Although acceptor limitation (as measured by Y(NA)) is elevated on initial increases in light intensities for the *fnr1* mutant (Figure 2), this is not the case for the *tic62/trol* mutant (Figure 3, Supplemental Figure S1) neither for *tic62/trol* or *fnr1*:Zm*FNR3* on sudden high light (Figure 4). Moreover, infiltration of leaves prior to measurement with MV, which eliminates acceptor limitation at PSI, does not immediately diminish the difference in tPm between these genotypes and the WT (Figure 5), suggesting that acceptor limitation is not the predominant cause of their increased PSI photoinactivation. The inhibition by MV later in the time course presumably arises from superoxide production, and it is interesting that it does not immediately impact on whatever protective function FNR is performing in sudden high light. This may be related to reports that MV is actually a relatively weak inhibitor of electron transfer by Fd between PSI and FNR (Setif, 2015), meaning that under the conditions used here sufficient reduced Fd is probably still available to FNR.

The increasing light experiments (Figures 2 and 3) were designed to distinguish damage at PSII from PSI in conditions where NPQ was able to develop, while the sudden light increase (Figure 4) tests PSI activity when electron flux from PSII is maximum. The stronger binding of FNR to the Tic62/TROL tether proteins in WT and *fnr1*:Zm*FNR1* lines at the onset of the high light period is therefore a more likely explanation for their higher tPm values than in *fnr1*, *tic62/trol* or *fnr1*:Zm*FNR3*, rather than differences in FNR abundance. The data indicate that, without NPQ, PSI acceptors are overwhelmed irrespective of any differences in FNR content seen between our genotypes. We included the *fnr1*:Zm*FNR1* plants in our study to examine whether tighter binding to membrane tethers might enhance PSI protection. In most experiments, this was not the case, but intriguingly
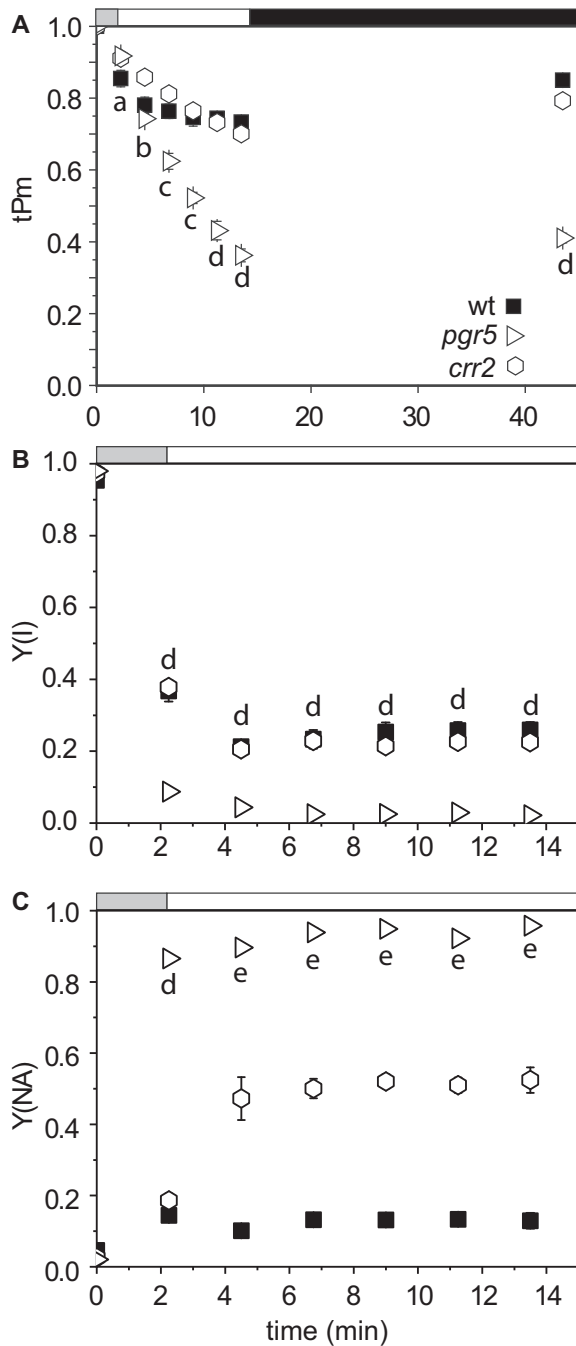
Figure 7 Examining the contribution of NDH and pgr5 mediated CEF to tPm protection in high light stress. P700 absorption and chlorophyll *a* fluorescence was assessed on *A. thaliana* genotypes: WT (black squares), *pgr*5 (open right-pointing triangles) and *crr*2 (open hexagons). Timing of changes in light intensity is indicated above the graph: the gray bar indicates a step-wise increase to first 543, then 692 μmol photon $m^{-2}s^{-1}$ (1 min each), the white bar indicates continuous illumination at 1,385 μmol photon $m^{-2}s^{-1}$, and the black bar indicates a dark relaxation period. A, tPm was measured over illumination and absolute Pm was determined after 30 min of dark adaptation. B, Effective quantum yield of PSI (Y(I)). C, acceptor limitation at PSI (Y(NA)). Data shown are means ± SEM ($n \geqslant 3$ individuals per genotype). Significant differences were attributed by post-hoc honestly significant difference Tukey's test and P values under 0.05 are indicated by are indicated as the following letters: "a" for *pgr*5 and *crr*2 ≠ WT; "b" for *pgr*5 and WT ≠ *crr*2; "c" for *pgr*5 ≠ *crr*2; "d" for *pgr*5 ≠ WT and *crr*2; "e" for *pgr*5 ≠ WT.
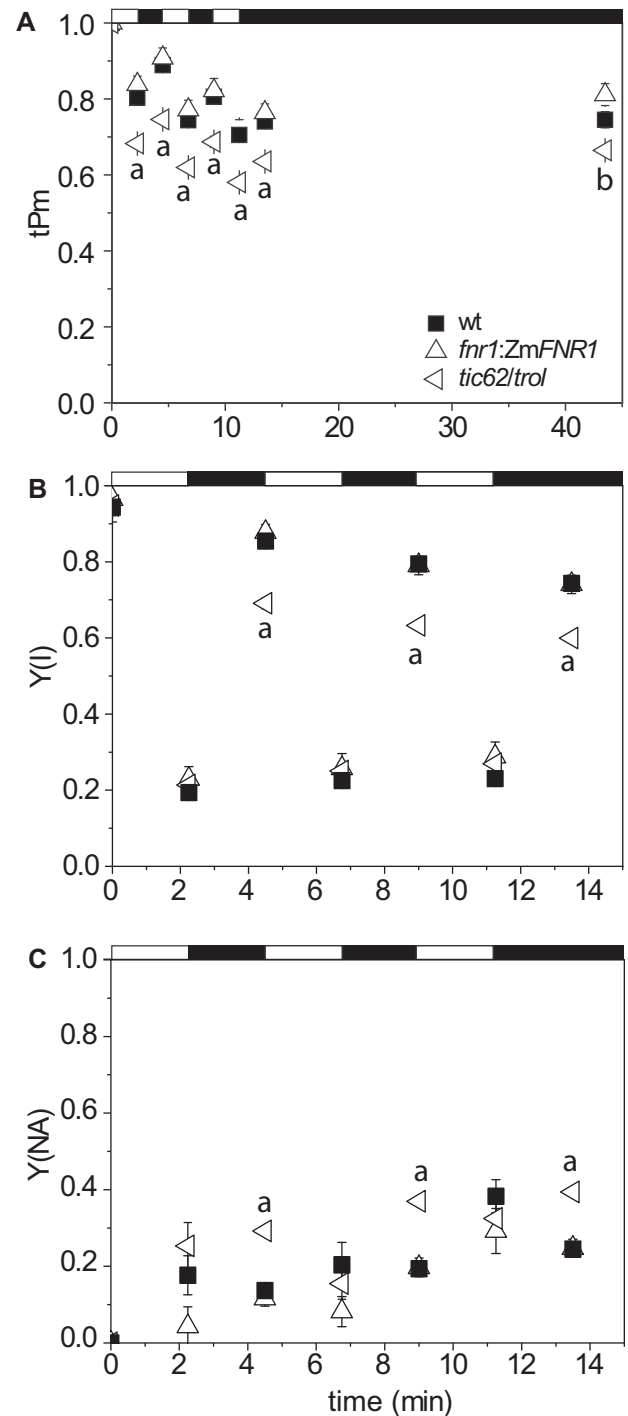
Figure 8 Impact of FNR:tether interactions on PSI inactivation during short-term light fluctuation. Timing of changes in light intensity is indicated above the graphs: black bars = darkness, while white bars = 1,385 μmol photon $m^{-2}s^{-1}$. P700 absorption and chlorophyll *a* fluorescence were followed in *A. thaliana* genotypes: WT (black squares), *fnr1*:Zm-*FNR1* (open upward-pointing triangles), and *tic62/trol* (open left-pointing triangles). A, tPm with absolute Pm determined after 30 min of dark adaptation following light treatment. B, Effective quantum yield of PSI (Y(I)). C, acceptor limitation at PSI (Y(NA)). Data shown are means ± SEM ($n \geqslant 3$ individuals per genotype). Significant differences were attributed by post-hoc honestly significant difference Tukey's test and are indicated by the following letters: "a" for *fnr1*:Zm-*FNR1* and WT ≠ *tic62/trol*; "b" for *fnr1*:Zm-*FNR1* ≠ *tic62/trol*.

fnr1:Zm*FNR1* did show slightly higher Pm values than the WT following dark recovery from the fluctuating light protocol (Figure 8).

As we previously reported an impact of FNR location on CEF during the dark to light transition for the *fnr1* and *fnr1*:Zm*FNR3* lines (in which FNR:membrane tether interactions are disrupted) (Kramer et al., 2021), we confirmed that this phenotype was also present in *tic62/trol* mutants (Figure 5A). The absence of this CEF might be expected to result in slower generation of ΔpH, which is indeed the case for this genotype (Figure 5B). We could not detect a significant difference in steady-state ΔpH, which might be expected as it is subject to extensive regulation (Tikkanen et al., 2015; Colombo et al., 2016; Yang et al., 2018). Many chloroplast protective mechanisms are dependent on ΔpH, including NPQ (Johnson and Ruban, 2011) and photosynthetic control (Colombo et al., 2016). We found no evidence for a relationship between NPQ and tPm or Y(I) in our genotypes (Figure 7; Supplemental Figure S3) and plants with enhanced or attenuated NPQ also showed minimum impact on PSI photoinactivation. This confirms previous reports that PSII downregulation has little effect on PSI protection (Tikkanen et al., 2015; Shimakawa and Miyake, 2018a, 2018b).

An inability to regulate electron donor supply by photosynthetic control has been proposed to cause the extreme PSI damage reported in *pgr5* mutants (Shimakawa and Miyake, 2018a, 2018b; Lima-Melo et al., 2019a, 2019b) and confirmed here (Figures 1 and 7). In this work, we did not compare the dark-adapted and light acclimated CEF capacity of *pgr5* and *crr2* plants, but the same technique has previously been used to show that, while NDH mutants are relatively unaffected, dark-adapted Arabidopsis *pgr5* mutants have decreased total CEF capacity, as measured following 120 s illumination (Suorsa et al., 2016). As the *tic62/trol* plants show lower rates of initial ΔpH generation (Figure 5, B and C), it seems likely that a slower induction of photosynthetic control might also be responsible for the PSI inactivation associated with decreased FNR content and membrane tether interaction.

Interestingly, during the first 5 min of high light stress, the tPm values for *pgr5* plants are higher than or equivalent to WT (Figure 1), and only decrease drastically thereafter. Those of *tic62/trol* and *fnr1*:Zm*FNR3* (Figure 4), and *fnr1* (Supplemental Figure S2) show the opposite trend, with an immediate drop relative to WT, after which the relative difference between the genotypes changes little. This is consistent with disruption of a process in the initial stages of illumination, such as the slower induction of ΔpH seen in Figure 5, B and C. FNR has been found in complex with PGR5 in algae (Iwai et al., 2010) and angiosperm PGRL1 was also reported to interact with FNR (DalCorso et al., 2008). AA is the canonical inhibitor of FQR-dependent CEF, and evidence supports a role for PGR5 in its mechanism of action (Sugimoto et al., 2013), while AA also abolishes FNR-dependent differences in tPm (Figure 5D). Although our data do not rule out these proteins acting in concert, they suggest that the mechanism disrupting

CEF induction during the dark to light transition is different between the *pgr5* mutant and the *fnr1*, *tic62/trol*, or *fnr1*:Zm*FNR3* genotypes.

One possible explanation for our data is therefore that, in addition to acceptor limitation, the stress phenotype associated with decreased FNR content and tether association could be due to increased donor arrival through slower induction of photosynthetic control. This would explain the specific, short-term inactivation of PSI seen in the *fnr1* and *tic62/trol* genotypes on exposure to high light.

Materials and methods

Plant material and growth conditions

Unless otherwise indicated, plants were grown in 12 h light at 21°C, 12 h dark at 18°C, and in 0.12 L pots on a 6:6:1 ratio of John Innes No. 3 soil, Levington M3 potting compost and perlite (Scotts UK, Ipswich, UK). Arabidopsis (*A. thaliana*) genotypes ecotype Columbia (WT) and *fnr1* were as described in (Hanke et al., 2008), Arabidopsis plants expressing *Zea mays FNR1*, *FNR2*, and *FNR3* in the *fnr1* background were as described previously (Kramer et al., 2021) and *tic62/trol* (Lintala et al., 2014) was a kind gift of Paula Mulo. *pgr5* (Munekage et al., 2002)) and *crr2* (Hashimoto et al., 2003) were a kind gift from Toshiharu Shikanai. The *npq4* (Havaux and Niyogi, 1999) and *L17* (Li et al., 2002) were also used in this work. Unless stated otherwise all measurements were carried out on 6-week-old plants that showed no signs of inflorescence or visible anthocyanin accumulation. Plants were dark-adapted for 45 min before each measurement and F_v/F_m was on average 0.78 ± 0.002 with no significant difference between genotypes.

Chlorophyll fluorescence and P700 absorption measurements and parameters

Chlorophyll *a* fluorescence and P700 oxidation measurements were performed simultaneously using a DUAL-KLAS-NIR-PAM (Walz, Effeltrich, Germany). In this method, the P700 redox state is monitored by deconvoluting the four absorption signals by differential model plots (Klughammer and Schreiber, 2008).

An assessment of the true quantity of photoinactivated PSII, as photochemical qPd, was calculated as described by Ruban and Murchie (2012).

$$qPd = (Fm' - Fo'_{act.})/(Fm' - Fo'_{calc.})$$

where Fm' is the maximum fluorescence yield after exposure to actinic light, $Fo'_{act.}$ and $Fo'_{calc.}$ are the actual and theoretical minimum fluorescence yields measured in the dark after actinic light treatment, respectively. $Fo'_{calc.}$ is determined according to the equation of Oxborough and Baker (1997), as defined below.

$$Fo'_{calc.} = 1/(1/Fo - 1/Fm + 1/Fm')$$

At lower actinic light levels, $Fo'_{act.} \approx Fo'_{calc.}$ and $qPd = 1$. However, as the intensity of actinic light rises, $Fo'_{act.}$ also increases, which is an indicator of photoinactivation. The

divergence between Fo′$_{act.}$ and Fo′$_{calc.}$ is due to permanent closure of RCs and causes qPd < 1.

The effective 'quantum yield' of PSII (Y(II) is undermined by two processes induced by excessive light: NPQ and photoinactivation (qPd). The effect of each upon Y(II) was therefore calculated as

$$Y(II) = (qPd \cdot Fv/Fm)/[1 + (1 - Fv/Fm) \cdot NPQ]$$

Fv/Fm represents the maximum Y(II), which is calculated as (Fm − Fo)/Fm, with Fo and Fm being the minimum and maximum fluorescence yields, respectively. The theoretical Y(II) for a given NPQ is calculated with maximal values of Fv/Fm and qPd as constants. Damage to PSI is usually quantified as a change in the maximum photo-oxidisible fraction of PSI (Pm), as measured following dark adaptation. According to Klughammer and Schreiber (2008), Pm can be determined during illumination by (1) measuring the maximal signal level induced by a saturating pulse (oxidisable P700), and (2) measuring the signal level in the dark several hundred milliseconds after the saturating pulse (baseline level; P700 fully reduced). In this work, we have combined these approaches to estimate activity of PSI during illumination. Actinic light is turned off, and far-red light is applied for 10 s before measurement of Pm with a saturating pulse. To avoid confusion, we refer to measurements following dark adaptation/recovery as Pm (photodamage), while values taken during illumination, from which PSI capacity partially recovers (Figure 1), are termed "transient Pm" or tPm, and reflect steady-state inactivation. Both Pm and tPm measurements were normalized to an initial Pm measured following 45-min dark adaptation prior to illumination. Y(I) and Y(NA) were calculated from the P700 traces according to published protocols (Klughammer and Schreiber, 2008). Typical WT chlorophyll fluorescence and P700 traces are shown in Supplemental Figure S5. For vacuum infiltration experiments, leaves of dark-adapted Arabidopsis plants were individually vacuum infiltrated by placing a whole leaf inside a syringe barrel containing 20 mL of buffer (330 mM sorbitol, 20 mM HEPES, pH 7) with or without AA (5 µM) or MV (250 µM). The narrow syringe opening was blocked and the plunger was used to gently draw air out of the tissue until the leaf lost buoyancy, at which point it was immediately measured.

Chloroplast extraction and proton gradient determination

The protocol was performed basically as described previously (Saccon et al., 2020a, 2020b). Briefly, Protoplasts were obtained from the mesophyll layer of dark-adapted leaves from Arabidopsis adult plants. To expose the chloroplast-enriched leaf layer to the enzyme solution, the lower epidermis was removed with adhesive tape. Leaves were then floated for 1 h on a solution containing 0.4 M Mannitol, 20 mM KCl, 20 mM MES, 10 mM CaCl$_2$, 0.1% bovine serum albumin (BSA) (pH 5.5) in the presence of 1.5% cellulase Onozuka^{TM} R-10 and 0.4% Macerozyme R-10 (Yakult, from Serva, Heidelberg, Germany). The solution was then filtered through a layer of muslin cloth and centrifuged twice (3 min, 100 rcf, 4 C). The obtained protoplasts were resuspended in reaction buffer containing 0.5 sorbitol, 20 mM HEPES, 20 mM MES, 20 mM Na-citrate, 10 mM NaHCO$_3$, 15 mM MgCl$_2$, 0.1% BSA (pH 8). Their intactness was checked with a bright-field optical microscope and Fv/Fm average values were confirmed.

ΔpH was determined from the measurement of 9-aminoacridine (9-AA) fluorescence using the Dual-ENADPH and Dual-DNADPH modules for the Dual-PAM-100 fluorimeter (Walz, Effeltrich, Germany). Intact chloroplasts (35 µM chlorophyll) were suspended in reaction buffer (as above) in the presence of 5 µM 9-AA. The chloroplasts were treated using 312 or 586 µmol photon m^{-2} s^{-1} actinic light for 5 min, followed by 5 min of darkness. The 9-AA quenching traces were normalized to (fluorescence before illumination − fluorescence after illumination)/fluorescence before illumination. Half time of ΔpH induction (t$_{1/2}$) was taken as the time for the fluorescence level to reach half of the maximum value of quenched fluorescence upon illumination.

CEF measurements

Measurements were performed basically as described previously (Kramer et al., 2021). In brief, plants were dark incubated for 30 min before transfer into actinic light at 150 µmol photon m^{-2} s^{-1}. After 20 s and 5 min of illumination, LEF and CEF were measured by following the relaxation kinetics of the carotenoid electrochromic bandshift at 520 nm (corrected with the bandshift at 546 nm). Saturating FR light (λ > 720 nm), was used to fully excite PSI with minimum excitation of PSII and calculate the CEF only signal. Electron flow was estimated from the amplitude of the electrochromic shift (ECS) signal upon excitation with a saturating single turnover flash (5 ns laser pulse). Total electron flow was measured with an actinic flash of 1,100 µmol photon m^{-2} s^{-1} while CEF was measured with only FR light at the maximum setting (estimated as 1,400 µmol photon m^{-2} s^{-1} by the manufacturer). LEF was calculated by subtraction of CEF from total electron flow.

FNR activity

Crude leaf extracts were prepared from 6-week-old plants by grinding with sand at 4°C in 50 mM Tris–HCl pH 7.5, 100 mM NaCl, 2 mM MgCl$_2$, 1 mM pefabloc, 0.1% w/v polyvinylpolypyrrolidone. The supernatant from a 2 min, 2,000 g centrifugation at 4°C was taken. FNR in this sample was solubilized by the addition of Triton X-100 to 1% (v/v), before further centrifugation at 15,000 g at 4°C for 5 min. FNR activity of this supernatant, equivalent to 30 µg total protein, was measured in the dark using a cytochrome c reduction assay in the presence of 20 µM Arabidopsis Fd 2 and an NADPH regeneration system as described previously (Hanke et al., 2005).

Statistics

The t test Student's, analysis of variance, and post-hoc analysis Tukey's tests were also performed in R version 3.5.3 (R_Core_Team, 2019).

Accession numbers

Supplemental data

The following materials are available in the online version of this article.

Supplemental Figure S1. The impact of FNR:tether interaction on PSI and PSII photoinactivation during increasing light intensity.

Supplemental Figure S2. Additional experiments on the impact of FNR:tether associations on PSI and PSII photoinactivation during high light exposure in Arabidopsis.

Supplemental Figure S3. Impact of altered NPQ on PSI inactivation over increasing light (A and B) and during sudden high light stress (C–E) in Arabidopsis.

Supplemental Figure S4. Impact of two different CEF pathways on photoinactivation of PSI and PSII during a gradual increase of light intensity.

Supplemental Figure S5. Example traces of the initial section of a typical PSII chlorophyll fluorescence (red trace) and P700 absorption (blue trace) simultaneous measurement.

Acknowledgments

Funding

Conflict of interest statement: The authors have no conflict of interest to declare.

References

Alboresi A, Storti M, Cendron L, Morosinotto T (2019) Role and regulation of class-C flavodiiron proteins in photosynthetic organisms. Biochem J **476**: 2487–2498

Allahverdiyeva Y, Ermakova M, Eisenhut M, Zhang P, Richaud P, Hagemann M, Cournac L, Aro EM (2011) Interplay between flavodiiron proteins and photorespiration in Synechocystis sp. PCC 6803. J Biol Chem **286**: 24007–24014

Allen JF, Hall DO (1974) The relationship of oxygen uptake to electron transport in photosystem I of isolated chloroplasts: the role of superoxide and ascorbate. Biochem Biophys Res Commun **58**: 579–585

Alte F, Stengel A, Benz JP, Petersen E, Soll J, Groll M, Bolter B (2010) Ferredoxin:NADPH oxidoreductase is recruited to thylakoids by binding to a polyproline type II helix in a pH-dependent manner. Proc Natl Acad Sci USA **107**: 19260–19265

Andersen B, Scheller HV, Moller BL (1992) The PSI-E subunit of photosystem I binds ferredoxin:NADP + oxidoreductase. FEBS Lett **311**: 169–173

Asada K (1999) THE WATER-WATER CYCLE IN CHLOROPLASTS: scavenging of active oxygens and dissipation of excess photons. Annu Rev Plant Physiol Plant Mol Biol **50**: 601–639

Benz JP, Lintala M, Soll J, Mulo P, Bolter B (2010) A new concept for ferredoxin-NADP(H) oxidoreductase binding to plant thylakoids. Trends Plant Sci **15**: 608–613

Burrows PA, Sazanov LA, Svab Z, Maliga P, Nixon PJ (1998) Identification of a functional respiratory complex in chloroplasts through analysis of tobacco mutants containing disrupted plastid ndh genes. EMBO J **17**: 868–876

Chaux F, Peltier G, Johnson X (2015) A security network in PSI photoprotection: regulation of photosynthetic control, NPQ and O2 photoreduction by cyclic electron flow. Front Plant Sci **6**: 875

Clark R, Hawkesford M, Coughlan S, Bennett J, Hind G (1984) Association of ferredoxin-NADP + oxidoreductase with the chloroplast cytochrome bf complex. FEBS Lett **174**: 137–142

Colombo M, Suorsa M, Rossi F, Ferrari R, Tadini L, Barbato R, Pesaresi P (2016) Photosynthesis control: an underrated short-term regulatory mechanism essential for plant viability. Plant Signal Behav **11**: e1165382

DalCorso G, Pesaresi P, Masiero S, Aseeva E, Schunemann D, Finazzi G, Joliot P, Barbato R, Leister D (2008) A complex containing PGRL1 and PGR5 is involved in the switch between linear and cyclic electron flow in Arabidopsis. Cell **132**: 273–285

Fisher N, Kramer DM (2014) Non-photochemical reduction of thylakoid photosynthetic redox carriers in vitro: relevance to cyclic electron flow around photosystem I? Biochim Biophys Acta **1837**: 1944–1954

Fufezan C, Rutherford AW, Krieger-Liszkay A (2002) Singlet oxygen production in herbicide-treated photosystem II. FEBS Lett **532**: 407–410

Hanawa H, Ishizaki K, Nohira K, Takagi D, Shimakawa G, Sejima T, Shaku K, Makino A, Miyake C (2017) Land plants drive photorespiration as higher electron-sink: comparative study of post-illumination transient O2 -uptake rates from liverworts to angiosperms through ferns and gymnosperms. Physiol Plant **161**: 138–149

Hanke GT, Endo T, Satoh F, Hase T (2008) Altered photosynthetic electron channelling into cyclic electron flow and nitrite assimilation in a mutant of ferredoxin:NADP(H) reductase. Plant Cell Environ **31**: 1017–1028

Hanke GT, Okutani S, Satomi Y, Takao T, Suzuki A, Hase T (2005) Multiple iso-proteins of FNR in Arabidopsis: evidence for different contributions to chloroplast function and nitrogen assimilation. Plant Cell Environ **28**: 1146–1157

Hashimoto M, Endo T, Peltier G, Tasaka M, Shikanai T (2003) A nucleus-encoded factor, CRR2, is essential for the expression of chloroplast ndhB in Arabidopsis. Plant J **36**: 541–549

Havaux M, Niyogi KK (1999) The violaxanthin cycle protects plants from photooxidative damage by more than one mechanism. Proc Natl Acad Sci USA **96**: 8762–8767

Hertle AP, Blunder T, Wunder T, Pesaresi P, Pribil M, Armbruster U, Leister D (2013) PGRL1 is the elusive ferredoxin-plastoquinone reductase in photosynthetic cyclic electron flow. Mol Cell **49**: 511–523

Hippler M, Drepper F (2006) Electron transfer between photosystem I and plastocyanin or cytochrome c6. *In* F Golbeck, ed, Photosystem I: The Light-Driven Plastocyanin: Ferredoxin Oxidoreductase. Springer, Dordrecht, Netherlands, pp 499–513

Huang W, Cai YF, Wang JH, Zhang SB (2018) Chloroplastic ATP synthase plays an important role in the regulation of proton motive force in fluctuating light. J Plant Physiol 226: 40–47

Ivanov AG, Morgan RM, Gray GR, Velitchkova MY, Huner NP (1998) Temperature/light dependent development of selective resistance to photoinhibition of photosystem I. FEBS Lett 430: 288–292

Iwai M, Takizawa K, Tokutsu R, Okamuro A, Takahashi Y, Minagawa J (2010) Isolation of the elusive supercomplex that drives cyclic electron flow in photosynthesis. Nature 464: 1210–1213

Johnson MP, Ruban AV (2011) Restoration of rapidly reversible photoprotective energy dissipation in the absence of PsbS protein by enhanced DeltapH. J Biol Chem 286: 19973–19981

Joliot P, Joliot A (2006) Cyclic electron flow in C3 plants. Biochim Biophys Acta 1757: 362–368

Juric S, Hazler-Pilepic K, Tomasic A, Lepedus H, Jelicic B, Puthiyaveetil S, Bionda T, Vojta L, Allen JF, Schleiff E, et al. (2009) Tethering of ferredoxin:NADP + oxidoreductase to thylakoid membranes is mediated by novel chloroplast protein TROL. Plant J 60: 783–794

Klughammer C, Schreiber U (2008) Saturation pulse method for assessment of energy conversion in PS I. PAM Appl Notes 1: 11–14

Kono M, Noguchi K, Terashima I (2014) Roles of the cyclic electron flow around PSI (CEF-PSI) and O(2)-dependent alternative pathways in regulation of the photosynthetic electron flow in short-term fluctuating light in Arabidopsis thaliana. Plant Cell Physiol 55: 990–1004

Kozuleva M, Goss T, Twachtmann M, Rudi K, Trapka J, Selinski J, Ivanov B, Garapati P, Steinhoff HJ, Hase T, et al. (2016) Ferredoxin:NADP(H) oxidoreductase abundance and location influences redox poise and stress tolerance. Plant Physiol 172: 1480–1493

Kozuleva MA, Petrova AA, Mamedov MD, Semenov AY, Ivanov BN (2014) O2 reduction by photosystem I involves phylloquinone under steady-state illumination. FEBS Lett 588: 4364–4368

Kramer M, Rodriguez-Heredia M, Saccon F, Mosebach L, Twachtmann M, Krieger-Liszkay A, Duffy C, Knell RJ, Finazzi G, Hanke GT (2021) Regulation of photosynthetic electron flow on dark to light transition by ferredoxin:NADP(H) oxidoreductase interactions. eLife 10: e56088

Krieger-Liszkay A (2005) Singlet oxygen production in photosynthesis. J Exp Bot 56: 337–346

Kudoh H, Sonoike K (2002) Irreversible damage to photosystem I by chilling in the light: cause of the degradation of chlorophyll after returning to normal growth temperature. Planta 215: 541–548

Leister D (2020) Alternative electron pathways in photosynthesis: strength in numbers. New Phytol 228: 1166–1168

Li XP, Muller-Moule P, Gilmore AM, Niyogi KK (2002) PsbS-dependent enhancement of feedback de-excitation protects photosystem II from photoinhibition. Proc Natl Acad Sci USA 99: 15222–15227

Lima-Melo Y, Alencar V, Lobo AKM, Sousa RHV, Tikkanen M, Aro EM, Silveira JAG, Gollan PJ (2019a) Photoinhibition of photosystem I provides oxidative protection during imbalanced photosynthetic electron transport in Arabidopsis thaliana. Front Plant Sci 10: 916

Lima-Melo Y, Gollan PJ, Tikkanen M, Silveira JAG, Aro EM (2019b) Consequences of photosystem-I damage and repair on photosynthesis and carbon use in Arabidopsis thaliana. Plant J 97: 1061–1072

Lintala M, Allahverdiyeva Y, Kangasjarvi S, Lehtimaki N, Keranen M, Rintamaki E, Aro EM, Mulo P (2009) Comparative analysis of leaf-type ferredoxin-NADP oxidoreductase isoforms in Arabidopsis thaliana. Plant J 57: 1103–1115

Lintala M, Allahverdiyeva Y, Kidron H, Piippo M, Battchikova N, Suorsa M, Rintamaki E, Salminen TA, Aro EM, Mulo P (2007) Structural and functional characterization of

ferredoxin-NADP + -oxidoreductase using knock-out mutants of Arabidopsis. Plant J 49: 1041–1052

Lintala M, Lehtimaki N, Benz JP, Jungfer A, Soll J, Aro EM, Bolter B, Mulo P (2012) Depletion of leaf-type ferredoxin-NADP(+) oxidoreductase results in the permanent induction of photoprotective mechanisms in Arabidopsis chloroplasts. Plant J 70: 809–817

Lintala M, Schuck N, Thormahlen I, Jungfer A, Weber KL, Weber AP, Geigenberger P, Soll J, Bolter B, Mulo P (2014) Arabidopsis tic62 trol mutant lacking thylakoid-bound ferredoxin-NADP + oxidoreductase shows distinct metabolic phenotype. Mol Plant 7: 45–57

Marco P, Elman T, Yacoby I (2019) Binding of ferredoxin NADP(+) oxidoreductase (FNR) to plant photosystem I. Biochim Biophys Acta Bioenerg 1860: 689–698

Munekage Y, Hashimoto M, Miyake C, Tomizawa K, Endo T, Tasaka M, Shikanai T (2004) Cyclic electron flow around photosystem I is essential for photosynthesis. Nature 429: 579–582

Munekage Y, Hojo M, Meurer J, Endo T, Tasaka M, Shikanai T (2002) PGR5 is involved in cyclic electron flow around photosystem I and is essential for photoprotection in Arabidopsis. Cell 110: 361–371

Nawrocki WJ, Bailleul B, Picot D, Cardol P, Rappaport F, Wollman FA, Joliot P (2019) The mechanism of cyclic electron flow. Biochim Biophys Acta Bioenerg 1860: 433–438

Nikkanen L, Toivola J, Trotta A, Diaz MG, Tikkanen M, Aro EM, Rintamaki E (2018) Regulation of cyclic electron flow by chloroplast NADPH-dependent thioredoxin system. Plant Direct 2: e00093

Oxborough K, Baker NR (1997) Resolving chlorophyll a fluorescence images of photosynthetic efficiency into photochemical and non-photochemical components—calculation of qP and F'v/F'm without measuring F'o. Photosynth Res 54: 135–142

Palatnik JF, Tognetti VB, Poli HO, Rodriguez RE, Blanco N, Gattuso M, Hajirezaei MR, Sonnewald U, Valle EM, Carrillo N (2003) Transgenic tobacco plants expressing antisense ferredoxin-NADP(H) reductase transcripts display increased susceptibility to photo-oxidative damage. Plant J 35: 332–341

Palatnik JF, Valle EM, Carrillo N (1997) Oxidative stress causes ferredoxin-NADP + reductase solubilization from the thylakoid membranes in methyl viologen-treated plants. Plant Physiol 115: 1721–1727

Rantala S, Lempiainen T, Gerotto C, Tiwari A, Aro EM, Tikkanen M (2020) PGR5 and NDH-1 systems do not function as protective electron acceptors but mitigate the consequences of PSI inhibition. Biochim Biophys Acta Bioenerg 1861: 148154

Rodriguez RE, Lodeyro A, Poli HO, Zurbriggen M, Peisker M, Palatnik JF, Tognetti VB, Tschiersch H, Hajirezaei MR, Valle EM, et al. (2007) Transgenic tobacco plants overexpressing chloroplastic ferredoxin-NADP(H) reductase display normal rates of photosynthesis and increased tolerance to oxidative stress. Plant Physiol 143: 639–649

Ruban AV (2016) Nonphotochemical chlorophyll fluorescence quenching: mechanism and effectiveness in protecting plants from photodamage. Plant Physiol 170: 1903–1916

Ruban AV (2017) Quantifying the efficiency of photoprotection. Philos Trans R Soc Lond B Biol Sci 372: 20160393

Ruban AV, Murchie EH (2012) Assessing the photoprotective effectiveness of non-photochemical chlorophyll fluorescence quenching: a new approach. Biochim Biophys Acta 1817: 977–982

Ruban AV, Wilson S (2020) The mechanism of non-photochemical quenching in plants: localisation and driving forces. Plant Cell Physiol 62: 1063–1072

Saccon F, Durchan M, Polívka T, Ruban AV (2020a) The robustness of the terminal emitter site in major LHCII complexes controls xanthophyll function during photoprotection. Photochem Photobiol Sci 19: 1308–1318

Saccon F, Giovagnetti V, Shukla MK, Ruban AV (2020b) Rapid regulation of photosynthetic light harvesting in the absence of minor antenna and reaction centre complexes. J Exp Bot 71: 3626–3637

Sacharz J, Giovagnetti V, Ungerer P, Mastroianni G, Ruban AV (2017) The xanthophyll cycle affects reversible interactions between PsbS and light-harvesting complex II to control non-photochemical quenching. Nat Plants **3**: 16225

Sarewicz M, Pintscher S, Pietras R, Borek A, Bujnowicz L, Hanke G, Cramer WA, Finazzi G, Osyczka A (2021) Catalytic reactions and energy conservation in the cytochrome bc1 and b6f complexes of energy-transducing membranes. Chem Rev **121**: 2020–2108

Schreiber U, Klughammer C (2009) New NADPH/9-AA module for the DUAL-PAM-100: description, operation and examples of application. PAM Appl Notes **2**: 1–13

Setif P (2015) Electron-transfer kinetics in cyanobacterial cells: methyl viologen is a poor inhibitor of linear electron flow. Biochim Biophys Acta **1847**: 212–222

Shikanai T, Endo T, Hashimoto T, Yamada Y, Asada K, Yokota A (1998) Directed disruption of the tobacco ndhB gene impairs cyclic electron flow around photosystem I. Proc Natl Acad Sci USA **95**: 9705–9709

Shimakawa G, Ishizaki K, Tsukamoto S, Tanaka M, Sejima T, Miyake C (2017) The liverwort, marchantia, drives alternative electron flow using a flavodiiron protein to protect PSI. Plant Physiol **173**: 1636–1647

Shimakawa G, Miyake C (2018a) Changing frequency of fluctuating light reveals the molecular mechanism for P700 oxidation in plant leaves. Plant Direct **2**: e00073

Shimakawa G, Miyake C (2018b) Oxidation of P700 ensures robust photosynthesis. Front Plant Sci **9**: 1617

Shimakawa G, Miyake C (2019) What quantity of photosystem I is optimum for safe photosynthesis? Plant Physiol **179**: 1479–1485

Shin M, Tagawa K, Arnon DI (1963) Crystallization of ferredoxin-tpn reductase and its role in the photosynthetic apparatus of chloroplasts. Biochem Z **338**: 84–96

Sonoike K (2011) Photoinhibition of photosystem I. Physiol Plant **142**: 56–64

Sonoike K, Terashima I, Iwaki M, Itoh S (1995) Destruction of photosystem I iron-sulfur centers in leaves of Cucumis sativus L. by weak illumination at chilling temperatures. FEBS Lett **362**: 235–238

Steen CJ, Morris JM, Short AH, Niyogi KK, Fleming GR (2020) Complex roles of PsbS and xanthophylls in the regulation of non-photochemical quenching in Arabidopsis thaliana under fluctuating light. J Phys Chem B **124**: 10311–10325

Storti M, Segalla A, Mellon M, Alboresi A, Morosinotto T (2020) Regulation of electron transport is essential for photosystem I stability and plant growth. New Phytol **228**: 1316–1326

Sugimoto K, Okegawa Y, Tohri A, Long TA, Covert SF, Hisabori T, Shikanai T (2013) A single amino acid alteration in PGR5 confers resistance to antimycin A in cyclic electron transport around PSI. Plant Cell Physiol **54**: 1525–1534

Suorsa M, Grieco M, Jarvi S, Gollan PJ, Kangasjarvi S, Tikkanen M, Aro EM (2013) PGR5 ensures photosynthetic control to safeguard photosystem I under fluctuating light conditions. Plant Signal Behav **8**: e22741

Suorsa M, Jarvi S, Grieco M, Nurmi M, Pietrzykowska M, Rantala M, Kangasjarvi S, Paakkarinen V, Tikkanen M, Jansson S, et al. (2012) PROTON GRADIENT REGULATION5 is essential for proper acclimation of Arabidopsis photosystem I to naturally and artificially fluctuating light conditions. Plant Cell **24**: 2934–2948

Suorsa M, Rossi F, Tadini L, Labs M, Colombo M, Jahns P, Kater MM, Leister D, Finazzi G, Aro EM, et al. (2016) PGR5-PGRL1-dependent cyclic electron transport modulates linear electron transport rate in Arabidopsis thaliana. Mol Plant **9**: 271–288

Takagi D, Ishizaki K, Hanawa H, Mabuchi T, Shimakawa G, Yamamoto H, Miyake C (2017) Diversity of strategies for escaping reactive oxygen species production within photosystem I among land plants: P700 oxidation system is prerequisite for alleviating photoinhibition in photosystem I. Physiol Plant **161**: 56–74

Takagi D, Miyake C (2018) PROTON GRADIENT REGULATION 5 supports linear electron flow to oxidize photosystem I. Physiol Plant **164**: 337–348

Takahashi M, Asada K (1988) Superoxide production in aprotic interior of chloroplast thylakoids. Arch Biochem Biophys **267**: 714–722

Telfer A, Bishop SM, Phillips D, Barber J (1994) Isolated photosynthetic reaction center of photosystem II as a sensitizer for the formation of singlet oxygen. Detection and quantum yield determination using a chemical trapping technique. J Biol Chem **269**: 13244–13253

Tikkanen M, Mekala NR, Aro EM (2014) Photosystem II photoinhibition-repair cycle protects Photosystem I from irreversible damage. Biochim Biophys Acta **1837**: 210–215

Tikkanen M, Rantala S, Aro EM (2015) Electron flow from PSII to PSI under high light is controlled by PGR5 but not by PSBS. Front Plant Sci **6**: 521

Tjus SE, Moller BL, Scheller HV (1998) Photosystem I is an early target of photoinhibition in barley illuminated at chilling temperatures. Plant Physiol **116**: 755–764

Twachtmann M, Altmann B, Muraki N, Voss I, Okutani S, Kurisu G, Hase T, Hanke GT (2012) N-terminal structure of maize ferredoxin:NADP$^+$ reductase determines recruitment into different thylakoid membrane complexes. Plant Cell **24**: 2979–2991

Vojta L, Caric D, Cesar V, Antunovic Dunic J, Lepedus H, Kveder M, Fulgosi H (2015) TROL-FNR interaction reveals alternative pathways of electron partitioning in photosynthesis. Sci Rep **5**: 10085

Ware MA, Belgio E, Ruban AV (2015) Comparison of the protective effectiveness of NPQ in Arabidopsis plants deficient in PsbS protein and zeaxanthin. J Exp Bot **66**: 1259–1270

Wilson S, Ruban AV (2019) Quantitative assessment of the high-light tolerance in plants with an impaired photosystem II donor side. Biochem J **476**: 1377–1386

Wilson S, Ruban AV (2020) Enhanced NPQ affects long-term acclimation in the spring ephemeral Berteroa incana. Biochim Biophys Acta Bioenerg **1861**: 148014

Yamamoto H, Shikanai T (2013) In planta mutagenesis of Src homology 3 domain-like fold of NdhS, a ferredoxin-binding subunit of the chloroplast NADH dehydrogenase-like complex in Arabidopsis: a conserved Arg-193 plays a critical role in ferredoxin binding. J Biol Chem **288**: 36328–36337

Yamori W, Makino A, Shikanai T (2016) A physiological role of cyclic electron transport around photosystem I in sustaining photosynthesis under fluctuating light in rice. Sci Rep **6**: 20147

Yang C, Hu H, Ren H, Kong Y, Lin H, Guo J, Wang L, He Y, Ding X, Grabsztunowicz M, et al. (2016) LIGHT-INDUCED RICE1 regulates light-dependent attachment of LEAF-TYPE FERREDOXIN-NADP+ OXIDOREDUCTASE to the thylakoid membrane in rice and Arabidopsis. Plant Cell **28**: 712–728

Yang YJ, Zhang SB, Huang W (2018) Chloroplastic ATP synthase alleviates photoinhibition of photosystem I in tobacco illuminated at chilling temperature. Front Plant Sci **9**: 1648

Zhang H, Whitelegge JP, Cramer WA (2001) Ferredoxin:NADP+ oxidoreductase is a subunit of the chloroplast cytochrome b6f complex. J Biol Chem **276**: 38159–38165